PAPER

Entanglement entropy and entanglement spectrum of $Bi_{1-x}Sb_x$ (1 1 1) bilayers

IOP Publishing Journal of Physics: Condensed Matter
J. Phys.: Condens. Matter **30** (2018) 125501 (8pp) https://doi.org/10.1088/1361-648X/aaaf54

Entanglement entropy and entanglement spectrum of $Bi_{1-x}Sb_x$ (1 1 1) bilayers

Marta Brzezińska, Maciej Bieniek, Tomasz Woźniak, Paweł Potasz and Arkadiusz Wójs

Department of Theoretical Physics, Faculty of Fundamental Problems of Technology, Wrocław University of Science and Technology, 50-370 Wrocław, Poland

E-mail: marta.a.brzezinska@pwr.edu.pl

Received 22 November 2017, revised 9 February 2018
Accepted for publication 14 February 2018
Published 28 February 2018

Abstract

We study topological properties of $Bi_{1-x}Sb_x$ bilayers in the (1 1 1) plane using entanglement measures. Electronic structures are investigated within multi-orbital tight-binding model and structural stability is confirmed through first-principles calculations. The topologically non-trivial nature of the bismuth bilayer is proved by the presence of spectral flow in the entanglement spectrum. We consider topological phase transitions driven by a composition change x, an applied external electric field in Bi bilayers and strain in Sb bilayers. Composition- and strain-induced phase transitions reveal a finite discontinuity in the entanglement entropy. This quantity remains a continuous function of the electric field strength, but shows a finite discontinuity in the first derivative. We relate the difference in behavior of the entanglement entropy to the breaking of inversion symmetry in the last case.

Keywords: topological insulators, entanglement, topological phase transitions

(Some figures may appear in colour only in the online journal)

1. Introduction

Exploring novel phases of quantum matter has gathered interest due to promising applications in the fields of spintronics and quantum computation [1–3]. Considerable effort has been devoted to searching candidate materials for topological insulators (TIs), a class of band insulators hosting gapless edge states and described by a $\mathbb{Z}_2$ topological invariant [4–6]. Boundary modes lead to two spin-polarized counter-propagating currents, which are immune to the backscattering in presence of non-magnetic disorder [1, 2]. For quantum dot geometry, orbital magnetization resulting from edge state circulation has also been shown to exhibit similar robustness [7]. Essential ingredients for quantum spin Hall (QSH) phase are the time-reversal symmetry and spin–orbit coupling (SOC). Strong SOC is characteristic of heavy elements and opens the non-trivial bulk band gap. Proposals of realizing the QSH insulator in two dimensions (2D) [4, 8–10] were followed by successful experimental observations, ranging from thickness-tunable quantum wells to honeycomb-like systems based on group-IV and group-V elements [11], and recently as thin films of insulators protected by crystalline symmetries [12, 13].

In particular, theoretical predictions have shown that a single Bi bilayer in the (1 1 1) plane manifests helical edge modes propagating in opposite directions [14–17] and subsequently it was confirmed by scanning tunneling microscopy measurements [18–20]. Moreover, protected 1D edge states were detected in Bi_2Se_3 thin films [21, 22] and at the interface between heterostructures Bi(1 1 1)/Bi_2Te_3 [23]. Robustness of topological properties of Bi(1 1 1) were recently discussed in [24–26]. Extensive studies have been carried out for few-layer Bi and Sb systems [27–30]. Pure Bi(1 1 1) films up to eight bilayers in thickness were shown to exhibit a stable QSH phase [15]. In the case of Sb(1 1 1), films with less than four bilayers are expected to be topologically trivial [31]. To induce transition between trivial and QSH insulating phases, appropriate structure modifications were proposed, including SOC variation in Bi [24, 32], strain in Sb [33, 34], effect of substrates [16] and perpendicular electric field for strained Sb [35].

Over the years, quantum entanglement has been recognized as a valuable tool to identify topological properties of

systems. Subtle non-local correlations inherent in topological states can be captured by bipartite entanglement measures [36, 37]. Given a composite system AB in a pure state described by $|\psi_{AB}\rangle \in \mathcal{H}_A \otimes \mathcal{H}_B$, the reduced density matrix corresponding to the subsystem A can be obtained by tracing out degrees of freedom related to the subsystem B, $\rho_A = \mathrm{Tr}_B|\psi_{AB}\rangle\langle\psi_{AB}|$. Commonly used in the context of quantum information is the von Neumann entanglement entropy, defined as $S_A = -\mathrm{Tr}\rho_A \log \rho_A$. Li and Haldane [38] suggested that the Schmidt decomposition of quantum many-body wave function can be regarded as a unique signature of topological phase and provides more information about the system than a single value of S_A. Several non-interacting models describing clean [39–46] as well as disordered systems [47–49] have been already analyzed through the entanglement spectrum. The non-trivial nature of the system is determined by the spectral flow of eigenvalues of the correlation matrix, which is an analogy to the edge states crossing the energy gap and connecting valence and conduction bands in the systems with open boundary conditions.

In this work, we study topological properties of $Bi_{1-x}Sb_x$ bilayer through entanglement measures. We examine electronic properties and structural stability of $Bi_{1-x}Sb_x$ bilayers, which is achieved by employing multi-orbital tight-binding model and density functional theory (DFT) calculations. Both infinite and semi-infinite systems are considered. We investigate entanglement entropy and entanglement spectrum for free-fermion systems and show that they can be treated as viable tools to characterize topological properties of realistic models of topological insulators. Furthermore, topological phase transitions as a result of composition change x, perpendicular electric field applied to Bi bilayers and strain in Sb bilayers are discussed.

2. Methodology

2.1. Tight-binding model

A single sheet of Bi and Sb rhombohedral crystal structures in the (1 1 1) direction can be seen as a buckled honeycomb lattice and is illustrated in figure 1. We follow a widely used terminology calling a single sheet by bilayer [14, 18], as it consists of two sublattices forming two layers spatially separated by a distance h.

To study electronic properties of ultrathin films, we employ an sp^3 tight-binding model developed in [50] for bulk bismuth and antimony, neglecting hoppings between bilayers as proposed in [14]. Interatomic hoppings are parametrized within the Slater–Koster approach [51] and atomic spin–orbit coupling $\lambda\vec{L}\cdot\vec{S}$. The Hamiltonian of the model reads

$$\begin{aligned} H_{TB} = &\sum_{i,\alpha,\sigma} E_{i\alpha} c^\dagger_{i\alpha\sigma} c_{i\alpha\sigma} + \sum_{i,\alpha,\sigma} V^{R,G}_{\mathrm{Field}} c^\dagger_{i\alpha\sigma} c_{i\alpha\sigma} \\ &+ \sum_{\substack{\langle ij\rangle \\ \alpha,\alpha',\sigma}} V_{\alpha\alpha'} c^\dagger_{i\alpha\sigma} c_{j\alpha'\sigma} + \sum_{\substack{\langle\langle ij\rangle\rangle \\ \alpha,\alpha',\sigma}} V''_{\alpha\alpha'} c^\dagger_{i\alpha\sigma} c_{j\alpha'\sigma} \\ &+ \frac{\lambda}{3}\sum_i (c^\dagger_{iz\downarrow} c_{ix\uparrow} - c^\dagger_{iz\uparrow} c_{ix\downarrow} + \mathrm{i} c^\dagger_{iz\uparrow} c_{iy\downarrow} \\ &+ \mathrm{i} c^\dagger_{iz\downarrow} c_{iy\uparrow} + \mathrm{i} c^\dagger_{ix\downarrow} c_{iy\downarrow} - \mathrm{i} c^\dagger_{ix\uparrow} c_{iy\uparrow}) + \mathrm{H.c.} \end{aligned} \quad (1)$$

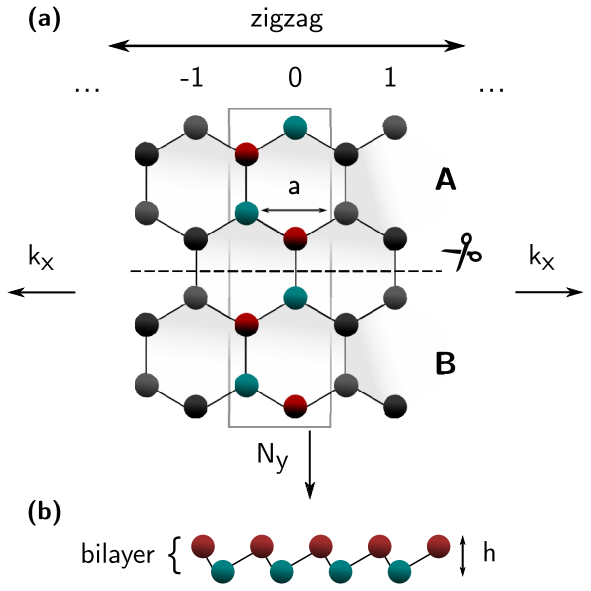

Figure 1. Lattice structure of Bi and Sb bilayer. (a) Top view of a ribbon with a zigzag edge termination of width N_y and periodic boundary conditions in x direction. Four atoms are within the unit cell of a ribbon. a the is lattice constant, 0 labels a unit cell, while -1 and 1 denote left and right neighboring cells, respectively. Red and green colors distinguish two sublattices forming a honeycomb lattice. The system can be divided into two halves A and B, with a cut marked by a dashed line, in order to evaluate entanglement measures. (b) Side view of a bilayer. h corresponds to the bilayer thickness.

where i,j are lattice indices (with $\langle\ldots\rangle$ and $\langle\langle\ldots\rangle\rangle$ denoting nearest and next-nearest neighbors, respectively), $\alpha = \{s, p_x, p_y, p_z\}$ labels orbitals and $\sigma = \{\uparrow,\downarrow\}$ spins. E_i corresponds to the on-site energies. $V_{\alpha\alpha'}$ ($V''_{\alpha\alpha'}$) are the hopping integrals between nearest (next-nearest) lattice sites (we keep this notation in order to be consistent with [50]). V_{Field} is a potential due to perpendicular electric field. In this case, atoms on two distinct sublattices are affected differently by the external field; on-site potentials of the atoms of two sublattices are different. The absolute value of the potentials on each sublattice does not matter, only their difference. Thus, without loss of generality, we can model its effect by adding potentials on two sublattices with opposite signs, $V^R_{\mathrm{Field}} = -V^G_{\mathrm{Field}}$, on $i \in R$ and $i \in G$ sites of two sublattices in a lattice indicated by red and green color in figure 1. The last term is the SOC with a strength λ. According to Chadi [52], 1/3 factor is introduced to renormalized atomic SOC in order to obtain correct SOC splitting of the valence band.

Similarities between Bi and Sb crystals can be seen by looking at Slater–Koster parameters listed in table 1, taken from [50]. Most of the parameters differ by less than 15%. The only significant change is in the spin–orbit coupling constant λ, 2.5 times larger in bismuth. Thus, a transition from QSH insulating phase to trivial insulator with increasing x in $Bi_{1-x}Sb_x$ is related, in general, to a decrease of spin–orbit coupling constant. While there can be some concerns related to application of the virtual crystal approximation (VCA), we note that more correct approach would require development of *ab initio* like tight-binding model, which is beyond the scope of our study. However, VCA is commonly used by

Table 1. Tight-binding parameters for Bi and Sb taken from [50, 15][a], [34][b]. d_1 denotes nearest-neighbor distance between sites in a honeycomb lattice.

Parameter (eV)	Bi	Sb	Parameter (eV)	Bi	Sb
E_s	−10.906	−10.068	$V_{pp\pi}$	−0.600	−0.582
E_p	−0.486	−0.926	$V''_{ss\sigma}$	0	0
$V_{ss\pi}$	−0.608	−0.694	$V''_{sp\sigma}$	0	0
$V_{sp\sigma}$	1.320	1.554	$V''_{pp\sigma}$	0.156	0.352
$V_{pp\sigma}$	1.854	2.342	$V''_{pp\pi}$	0	0
λ	1.5	0.6			
a (Å)	4.53	4.30	h (Å)	1.58[a]	1.64[b]
d_1 (Å)	3.062	2.902			

other authors, giving also the results in good agreement with the experiment, see [53].

2.2. DFT stability calculations of $Bi_{1-x}Sb_x$ alloys

We investigate the stability of $Bi_{1-x}Sb_x$ alloys with different composition x. This requires consideration a supercell of one of the monocrystals with one or more atomic sites replaced by the other compound. $3 \times 3 \times 1$ supercells were used for modeling of $Bi_{1-x}Sb_x$ mixed crystals. We have modeled $Bi_{0.72}Sb_{0.28}$ and ($Bi_{0.28}Sb_{0.72}$) mixed crystals with the last two alloys corresponding to 13 Bi(Sb) and 5 Sb(Bi) atoms in an 18 atoms unit cell. We note that such a choice of composition allows us to verify stability of the crystal around 25% with a more irregular atomic substitution in a supercell, which can better confirm the structure stability for arbitrary value of x. We note that more detailed analysis of the $Bi_{1-x}Sb_x$ crystal stability would require analysis of all possible configurations of Sb atoms in large unit cells, comparison of their total energies and choosing the lowest ones for every composition x. These computationally demanding studies are not strictly related to the subject of this work.

DFT calculations have been performed in ABINIT software [54] using the LDA exchange–correlation functional. The Bi and Sb atoms were modelled by fully relativistic PAW sets. The plane wave basis cut-off was 20 Ha and the Monkhorst–Pack k-point grid was set to $10 \times 10 \times 1$. The structures were fully relaxed until the interatomic forces were lower than 10^{-8} Ha/Bohr. The phonon calculations were performed in Phonopy software [55] which implements the Parlinski–Li–Kawazoe method that is based on the supercell approach with the finite displacement method [56]. Phonon band structures were calculated along Γ-M-K-Γ path in the reciprocal space. The supercells of given size are commensurate with all the q-vectors of the high symmetry points in a hexagonal Brillouin zone (BZ) [57].

Phonon dispersions for $Bi_{0.72}Sb_{0.28}$ and $Bi_{0.28}Sb_{0.72}$ mixed crystals are shown in figure 2. The multiple phonon branches are the consequence of folding of the phonon states in the supercell first BZ. We observe no imaginary phonon modes, which confirms the structural stability. We have also verified structural stability of $Bi_{0.5}Sb_{0.5}$ crystals (not shown here), in agreement with recent results presented in [58]. Thus, we confirmed that mixed $Bi_{1-x}Sb_x$ 2D bilayers are stable, at least for some of different compositions x, which was shown before only for bulk 3D materials.

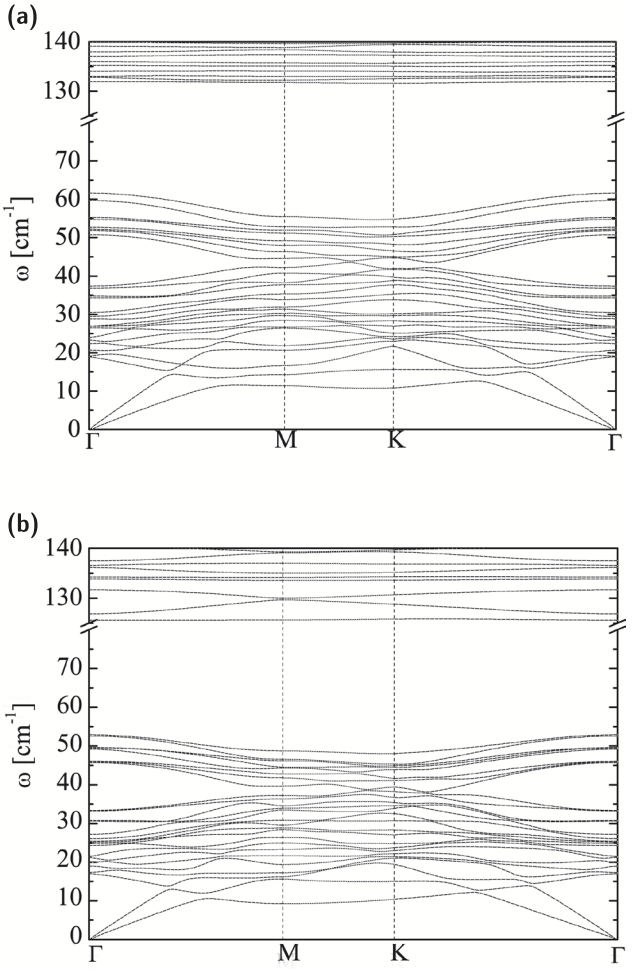

Figure 2. Phonon dispersion of (a) $Bi_{0.28}Sb_{0.72}$ and (b) $Bi_{0.72}Sb_{0.28}$ mixed crystals. Lack of modes with imaginary frequencies indicates stability of the crystals.

2.3. Entanglement measures for free-fermion systems

Quantum correlations between parts of the composite system can be studied quantitatively by means of entanglement measures [59]. Suppose the system is bipartited into two equal spatial parts, A and B, as in figure 1(a). Information about the part A is encoded into reduced density matrix ρ_A. In particular,

ρ_A can be represented as $\rho_A = \mathrm{e}^{-H_A}/Z_A$, with $Z_A = \mathrm{Tr}\left(\mathrm{e}^{-H_A}\right)$ being the partition function. The matrix H_A can be identified as the entanglement Hamiltonian and defined as a logarithm of thermal reduced density matrix at the fictitious temperature $T = 1$, $H_A = -\log \rho_A + c$, where c is a normalization constant. Therefore, the entanglement spectrum is defined as a set of eigenvalues of H_A denoted by $\{\xi\}$.

Entanglement measures for free fermionic lattice systems can be computed from the two-point correlation function restricted to the subsystem [60]

$$C_{ij}^{\alpha\beta} = \mathrm{Tr}\left(\rho_A c_{i\alpha}^{\dagger} c_{j\beta}\right), \tag{2}$$

where i,j are lattice indices within the subsystem A and α,β label orbitals or spins. If system is translationally-invariant, the Hamiltonian H can be written in the momentum space with the many-body ground state in a form $|GS\rangle = \prod_{n,k} a_{nk}^{\dagger}|0\rangle$ with operators $a_{nk}^{\dagger}$ corresponding to creation a particle with momentum k and n running over the occupied single-particle Bloch states. The Hamiltonian decouples into irreducible representations labeled by the conserved momentum k and can be diagonalized independently for each k value. Hence, the correlation matrix can be evaluated via formula $C_{ij}^{\alpha\beta}(k) = \langle GS|c_{i\alpha k}^{\dagger} c_{j\beta k}|GS\rangle$, where k labels different momentum sectors, but is not a basis transformation index. $C(k)$ is a Hermitian matrix and can be regarded as a spectrally flattened physical Hamiltonian with eigenvalues (denoted by $\{\zeta_k\}$) falling between 0 and 1. Most of the eigenvalues in the spectrum of $C(k)$ lie exponentially close to either 1 or 0, depending whether bulk states are fully localized in the subsystem A or B, respectively, and do not contribute to the entanglement entropy. However, states crossing the partition boundary give rise to non-zero entanglement entropy. If the Hamiltonian describes a topologically non-trivial Z_2 phase in 2D, $C(k)$ will reveal the spectral flow associated with continuous set of intermediate eigenvalues [42, 46]. A relation between $\{\zeta_k\}$ and the spectrum of $H_A(k)$ labeled by $\{\xi_k\}$ is following

$$\zeta_k = \left(1 + \mathrm{e}^{\xi_k}\right)^{-1}. \tag{3}$$

Due to this one-to-one correspondence, we refer to eigenvalues of the correlation matrix as the single-particle entanglement spectrum, which is a conventional practice in the literature [42, 45, 46]. Entanglement entropy [61, 62] is given by

$$S_A = -\sum_a \left(\zeta_a \log \zeta_a + (1-\zeta_a)\log\left(1-\zeta_a\right)\right), \tag{4}$$

where a is index running over all eigenvalues of C. S_A can be calculated [63] by summing over the entanglement entropy for each k-point with a normalization factor being the number of unit cells $S_A = 1/N_y \sum_k S_A(k)$.

It was also shown that the trace of C corresponding to the subsystem A called trace index is equivalent to the topological invariants for AII and A symmetry classes [45, 64]. Counting the discontinuities in the trace index provides a method to extract $\mathbb{Z}_2$ invariant. Physical edge states in the bulk gap that cross the Fermi level translate into discontinuities in the $\mathrm{Tr}\, C(k)$, thus trace index would not be applicable in the absence of boundary modes.

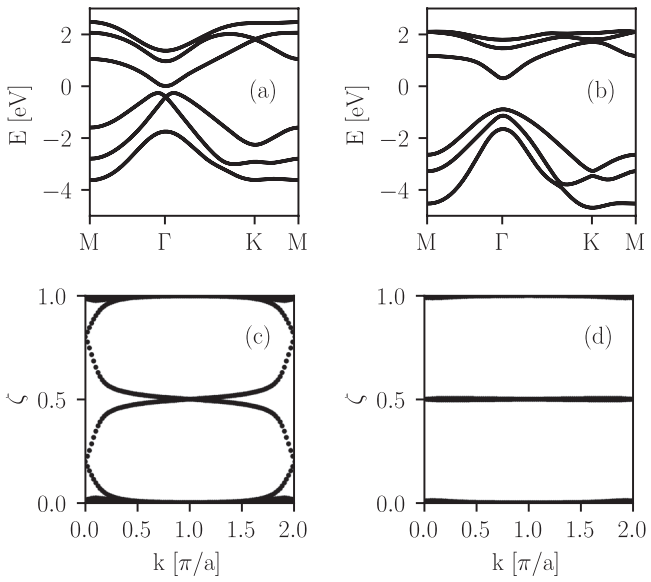

Figure 3. Energy band structures of (a) Bi and (b) Sb infinite bilayers. (c) and (d) are corresponding entanglement spectra, with an evidence of non-trivial topology of Bi seen as a spectral flow, not exhibited for Sb.

3. Entanglement spectra of pure Bi and Sb

3.1. Bi and Sb infinite bilayers

In figures 3(a) and (b) energy band structures of Bi and Sb infinite bilayers are shown. Both materials have well-defined band energy gaps around the Γ point. Two band structures are inverted with respect to each other. The concept of topological band inversion is usually confirmed by comparing orbital composition at a high-symmetry point in the BZ. In the case of bismuth and antimony, both conduction and valence band are made mostly from p orbitals. Here, the SOC-driven band inversion can be determined by measuring the degree of mismatch between the occupied band projection operators with and without SOC by the so-called spin–orbit spillage, see [65]. We determine topological properties by calculating the $\mathbb{Z}_2$ invariant for inversion-symmetric systems, according to the method from [6]. The non-trivial topology of Bi is confirmed as well by observation of the spectral flow in the entanglement spectrum of the reduced 1D BZ along the cut of the system into two parts, shown in figure 3(c). This feature is not manifested in the case of Sb, which indicates its trivial nature in figure 3(d).

3.2. Bi and Sb in a ribbon geometry

We consider a system in a ribbon geometry with periodic boundary conditions in x direction, where N_y denotes a width of the strip. Calculations are performed for the systems with $N_{\mathrm{at}} = 48$ atoms. We divide the system into two parts with a

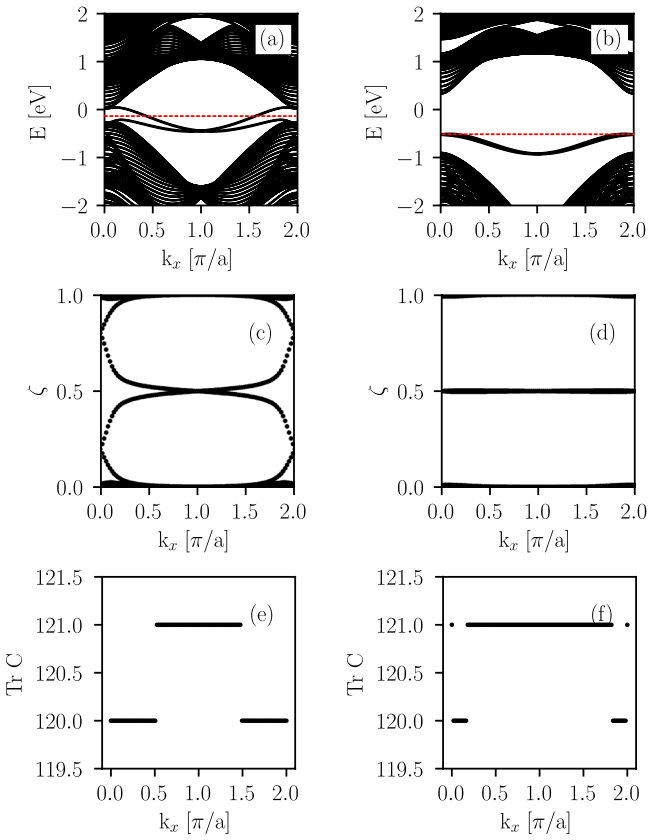

Figure 4. (a) and (b) Energy spectra near the Fermi level, (c) and (d) the corresponding single-particle entanglement spectra, and (e) and (f) trace indices for bismuth (left panel) and antimony (right panel) ribbons, respectively. The Fermi level is marked by red dotted lines.

cut parallel to the physical edges as depicted in figure 1(a). The considered system size ensures that two opposite edges of the system are sufficiently far that no hybridization between potential edge states is expected and edge modes would be perfectly confined within the subsystems.

Figure 4 compares energy spectra in the vicinity of the Fermi level ((a) and (b)), single-particle entanglement spectra ((c) and (d)) and trace indices ((e) and (f)) of Bi and Sb zigzag ribbons, respectively. We look at the features characteristic of non-trivial and trivial phases. Edge states spectrally connecting the conduction and valence bands are observed in the Bi bilayer, figure 4(a), which is typical of the TI regime. It is in contrast to almost flat-band edge states in Sb exhibited in the middle of the energy band gap and presented in figure 4(b). Entanglement spectra for a zigzag ribbon do not differ in comparision to the infinite case in figures 3(c) and (d). It was shown in [46] that the entanglement spectrum of the subsystem is strictly related to the energy spectrum of the spectrally flattened Hamiltonian with open boundary conditions. Thus, the presence of the edge states in the energy gap of the energy spectrum is revealed in entanglement spectra, in both nontrivial figure 4(c) and trivial figure 4(d) cases. We note that $\zeta = 0.5$ values mid-gap states in entanglement spectra are associated with the inversion symmetry present in the system.

We highlight that Bi armchair ribbons posses an extra pair of edge states in the energy gap, which lead to spurious modes in the single-particle entanglement spectra, but the subsequent conclusions would remain the same for both edge terminations. Topological properties can be also determined by counting the number of trace discontinuities in half the BZ *mod* 2, which is related to $\mathbb{Z}_2$ invariant [45]. In figure 4(e) there is only one jump discontinuity by 1 in $k_x \in [0, \pi]$, which leads to nontrivial topological invariant $\mathbb{Z}_2 = 1$. On the contrary, two discontinuities in half the BZ are noticed in figure 4(f), hence $\mathbb{Z}_2 = 0$.

4. Topological phase transitions

4.1. Composition-induced phase transition in $Bi_{1-x}Sb_x$

We investigate the transition to a trivial phase as the composition of antimony in $Bi_{1-x}Sb_x$ alloy increases. We consider a system in a torus geometry by applying periodic boundary conditions to the ribbon presented in figure 1(a) also along the y direction. Dividing the system into two spatial parts introduces two boundaries and results in a spectral symmetry as all the single-particle entanglement spectra eigenvalues come in pairs [66]. Three different size systems are examined: $N_y = 7, 10, 13$, corresponding to $N_{\text{at}} = 28, 48, 52$ atoms, respectively. Using virtual crystal approximation, we effectively change the values of hopping integrals between all lattice sites $t_x = (1 - x) \cdot t_{\text{Bi}} + x \cdot t_{\text{Sb}}$, where $t_{\text{Bi/Sb}}$ are parameters from table 1.

Firstly, we look at the dependence of the energy band gap at $k = 0$ on the alloy composition, shown in figure 5(a). The energy gap of pure Bi ($x = 0$) is $E_{\text{gap}} = 0.3$ eV. Finite-size effects are noticed in the range of small amounts of antimony as a kink in the energy gap evolution around $x \sim 0.12$ for a system with $N_{\text{at}} = 28$. The energy gap decreases with an increase of Sb concentration x and closes at $x = 0.243$ regardless of the system size. It reopens again as the system transits from TI to a trivial phase and increases linearly up to $E_{\text{gap}} = 1.2$ eV for pure Sb. The band gap closing point corresponds to topological phase transition and is in an agreement with calculations done for infinite 2D crystal. We note that single-particle ES for different Sb composition x before and after phase transition (not shown here) do not differ qualitatively in comparison to pure Bi and Sb in figures 3(c) and (d).

Figure 5(b) presents dependence of the entanglement entropy of subsystem A, S_A, of the antimony composition in $Bi_{1-x}Sb_x$ alloy. Pure Bi is characterized by the largest value of the entanglement entropy, which decreases monotonically with x. A discontinuity at $x = 0.243$ is observed for all system sizes and coincides with the energy band gap closing point seen in figure 5(a). After topological phase transition, the entanglement entropy S_A still decreases to its minimal value for pure Sb.

4.2. Electric field-driven topological phase transition in Bi bilayer

We apply an external electric field perpendicular to a pure Bi bilayer and observe whether distinct features are observed in the entanglement entropy and single-particle ES. An increase

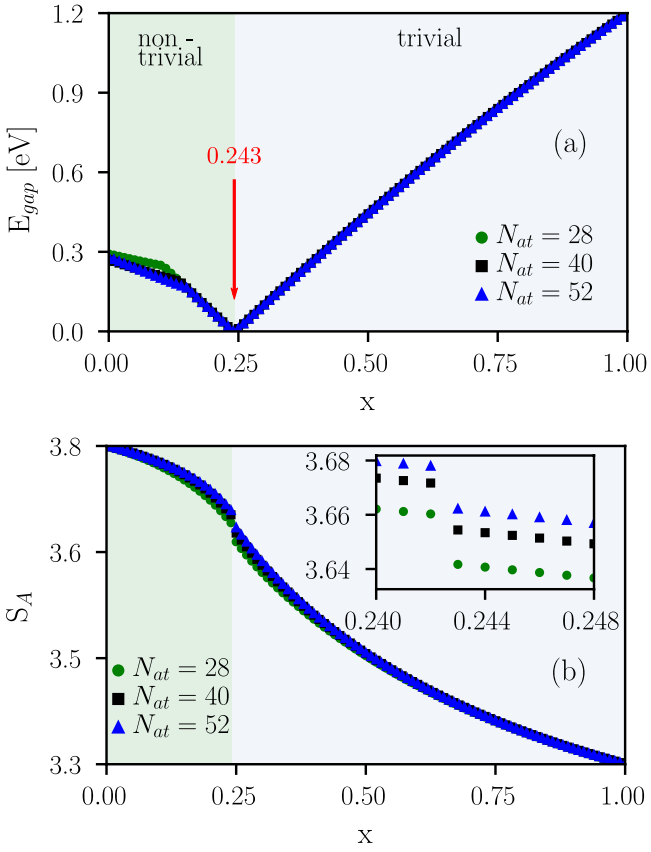

Figure 5. (a) Band gap evolution at the $k = 0$ point and (b) entanglement entropy as a function of antimony composition in $Bi_{1-x}Sb_x$. The red arrow in (a) indicates the band gap closing point. Different background colors refer to non-trivial/trivial regime. The inset in (b) zooms into discontinuity of S_A.

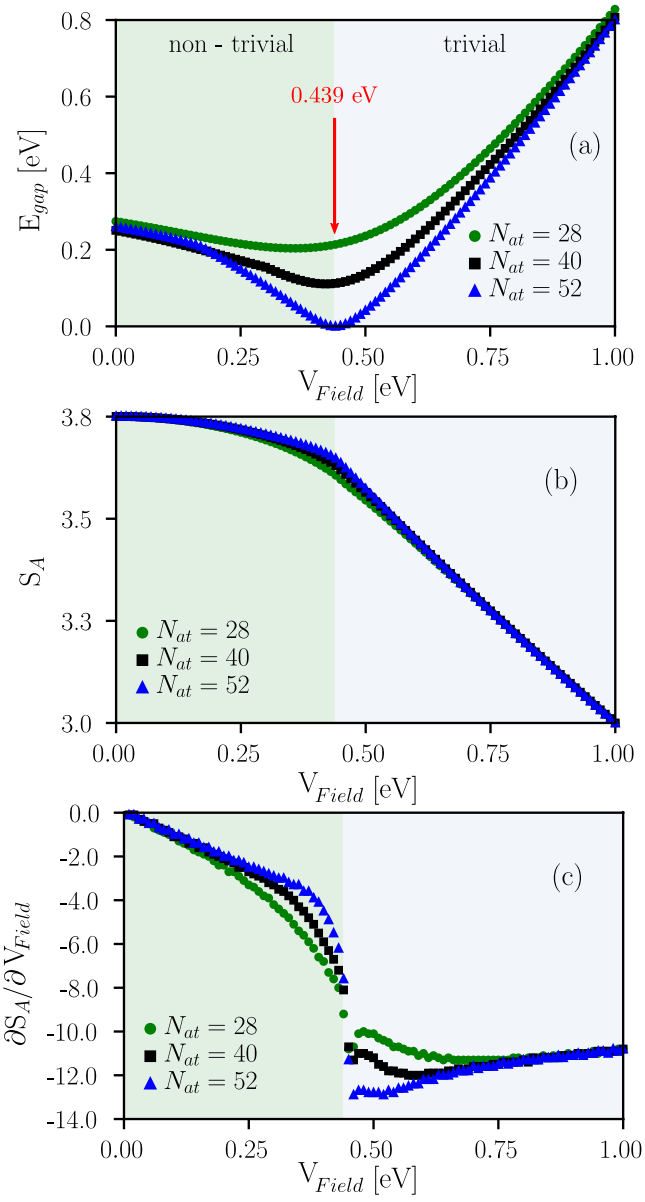

Figure 6. (a) Band gap evolution at the $k = 0$ as a function of external potential V_{Field}. For a sufficiently wide system, the band gap closes at $V_{\text{Field}} = 0.439$ eV, which is indicated by a red arrow. (b) Entanglement entropy as a function of external potential and (c) derivative of S_A with respect to V_{Field}. The derivative of the entanglement entropy becomes discontinuous at $V_{\text{Field}} = 0.439$ eV.

in V_{Field} leads to the energetic separation between two sublattices and acts similar to staggered potential in the Kane–Mele model [67].

In figure 6(a), the energy band gap as a function of external potential V_{Field} is plotted. The energy band gap does not close completely due to the finite size effects even for a very wide torus with $N_{\text{at}} = 52$ atoms, but entanglement measures are able to detect when topological phase transition should occur. In the thermodynamic limit, the band gap closes at $V_{\text{Field}} = 0.439$ eV.

Figure 6(b) presents the entanglement entropy and (c) its first derivative with respect to V_{Field}. Entanglement entropy is a continuous function of V_{Field}, while $\partial S_A/\partial V_{\text{Field}}$ is not. An inflection point in the entanglement entropy can be seen and corresponds to the band gap closure for the infinite system. The point is more clear as we increase the system size, as sharpness of the discontinuity in the derivative is strongly size-dependent. S_A decreases rapidly with the electric field after the phase transition. In the large V_{Field} limit the entanglement entropy saturates to almost zero value (not shown here) as the states are fully localized on the lattice sites. This is related to the fact that increase of the electric field weakens effectively the interatomic interactions described by hopping integrals and the effect of SOC, which are responsible for the entanglement. In the large electric field limit, the energy scale of hopping integrals and SOC are relatively negligible, and in consequence there is no entanglement between two parts of the system.

We look also at single-particle entanglement spectra for different values of the V_{Field}, shown in figure 7(a) before (for $V_{\text{Field}} = 0.24$ eV) and (b) after (for $V_{\text{Field}} = 0.54$ eV) phase transition. It differs significantly comparing to pure Bi and Sb. For small values of V_{Field}, initially two-fold degenerate spectrum splits into two sets of branches as illustrated in figure 7(a). After the phase transition to a trivial phase, the spectral flow is no longer exhibited, figure 7(b). Furthermore, there are no more mid-gap states at $\zeta = 0.5$, which indicates breaking of the inversion symmetry. For $V_{\text{Field}} \to \infty$ the single-particle entanglement spectra consist only of 0's and 1's, which corresponds to the non-interacting atomic limit.

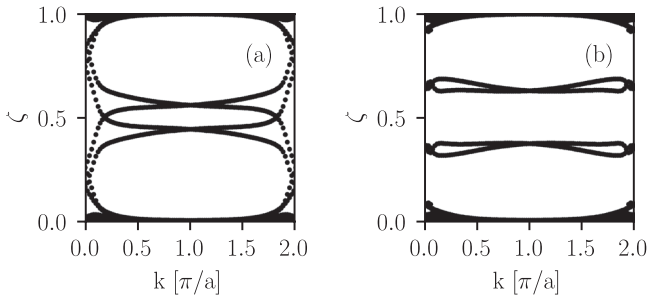

Figure 7. Single-particle entanglement spectra (a) before, for $V_{\text{Field}} = 0.24$ eV, and (b) after, for $V_{\text{Field}} = 0.54$ eV, topological phase transition.

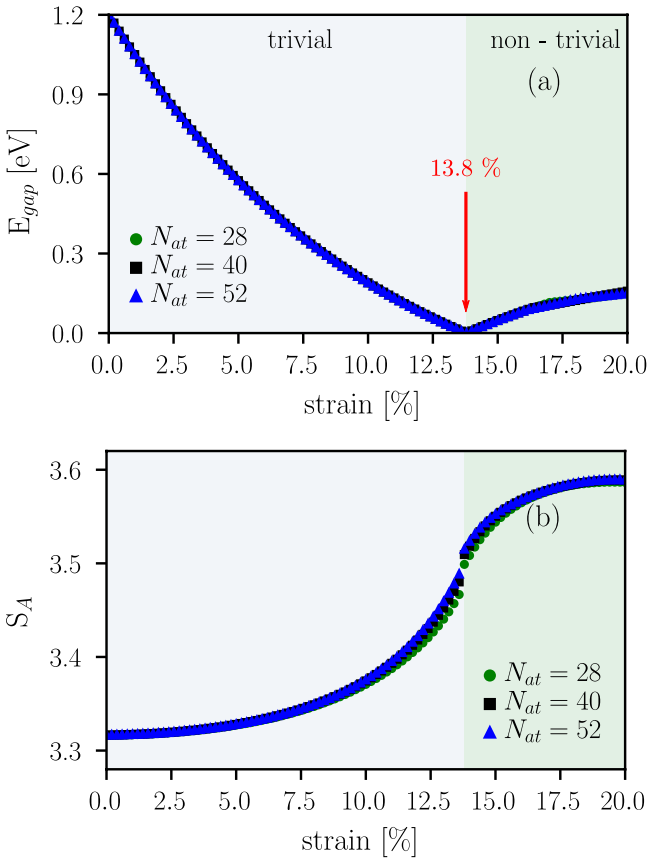

Figure 8. (a) Band gap evolution at $k = 0$ with respect to strain. The band gap closes at 13.8%. (b) Entanglement entropy as a function of strain.

4.3. Strain-induced topological phase transition in the Sb bilayer

We consider a strain-induced phase transition in the Sb bilayer. A strain is modeled by scaling hopping integrals due to a change of bond lengths and angles. Following Harrison [68], the value of the hopping parameter $V_{\alpha\beta}$ is modified as $V_{\alpha\beta} = V^0_{\alpha\beta} \cdot (d/d_0)^{-n}$, where $V^0_{\alpha\beta}$ corresponds to values for the unstrained case from table 1, while d and d_0 are new and unmodified bond lengths, respectively. Here, we investigate $n = 8$ in order to enhance the effect of V_{ij} strength modification.

In figure 8(a), the band gap evolution at $k = 0$ as a function of strain is presented. The band gap decreases with a strain strength and closes at the critical value 13.8% of strain. Originally a trivial antimony bilayer undergoes the topological phase transition with the bond lengthening. Since strain affects all hopping integrals between lattice sites, the inversion symmetry is preserved. Similar to the composition-induced phase transition, a small discontinuity in the entanglement entropy in figure 8(b) coincides with the band gap closing point. Also, the structure of single-particle entanglement spectra before and after phase transition is almost the same as those presented in figures 3(c) and (d) (not shown here).

5. Summary and discussion

To conclude, we have examined 2D $Bi_{1-x}Sb_x$ bilayers. We have confirmed their structural stability for different composition x by calculations of phonon dispersion within a DFT framework. We have shown that $Bi_{0.28}Sb_{0.72}$ and $Bi_{0.72}Sb_{0.28}$ thin films are structurally stable, in addition to pure bismuth and antimony bilayers, as well as $Bi_{0.5}Sb_{0.5}$, already discussed in the literature. Next, we have used entanglement entropy and entanglement spectrum to determine their topological properties and analyze topological phase transition. It has been shown that single-particle entanglement measures can provide supplemental information on topological properties of a system compared to electronic structure studies. We have shown that entanglement spectrum of topologically nontrivial Bi reveals a spectral flow, which is not present in trivial Sb. By considering a system in a ribbon geometry, we have shown also that topological properties of the system can be determined by looking at the trace index in half the BZ, which exhibit a single jump (odd) in a case of TI or two jumps (even) in a trivial case.

We have analyzed also phase transitions between topologically non-trivial/trivial phase driven by antimony composition x in $Bi_{1-x}Sb_x$, due to applied electric field in pure Bi, and strain in pure Sb. A phase transition resulting in a composition change occurs at $x = 24.3\,\%$, which differs from a TI regime in 3D bulk $Bi_{1-x}Sb_x$, reported for x ranging from 7% to 22% [6]. We point out that in 3D the band inversion process occurs at the L point in the BZ, which maps onto $\bar{M}$ point on the surface, while the band gap is observed at the Γ point in 2D. Composition- and strain-induced phase transitions reveal a finite discontinuity in the entanglement entropy. In the case of electric field, a phase transition seems to have a different character as entanglement entropy remains a continuous function of the electric field strength, while its first derivative is discontinuous. We relate this difference to the breaking of inversion symmetry in the last case. We do not qualify whether we observe the first and second order phase transitions, respectively, as this requires more careful analysis, including behavior of correlation length at a phase transition point and we leave it for a further work.

Acknowledgments

The authors were supported by National Science Center (NCN) of Poland, grant Sonata No. 2013/11/D/ST3/02703.

The use of resources of the Wrocław Centre for Networking and Supercomputing (WCSS) and Interdisciplinary Centre for Mathematical and Computational Modelling (ICM), grant No. G65-2 is kindly acknowledged.

ORCID iDs

Marta Brzezińska https://orcid.org/0000-0003-0657-4382
Paweł Potasz https://orcid.org/0000-0001-8383-2205

References

[1] Hasan M Z and Kane C L 2010 *Rev. Mod. Phys.* **82** 3045
[2] Qi X-L and Zhang S-C 2011 *Rev. Mod. Phys.* **83** 1057
[3] Nayak C, Simon S H, Stern A, Freedman M and Das Sarma S 2008 *Rev. Mod. Phys.* **80** 1083
[4] Kane C L and Mele E J 2005 *Phys. Rev. Lett.* **95** 146802
[5] Schnyder A P, Ryu S, Furusaki A and Ludwig A W W 2008 *Phys. Rev.* B **78** 195125
[6] Fu L and Kane C L 2007 *Phys. Rev.* B **76** 045302
[7] Potasz P and Fernández-Rossier J 2015 *Nano Lett.* **15** 5799
[8] Bernevig B A and Zhang S-C 2006 *Phys. Rev. Lett.* **96** 106802
[9] Bernevig B A, Hughes T L and Zhang S-C 2006 *Science* **314** 1757
[10] Liu C, Hughes T L, Qi X-L, Wang K and Zhang S-C 2008 *Phys. Rev. Lett.* **100** 236601
[11] Ren Y, Qiao Z and Niu Q 2016 *Rep. Prog. Phys.* **79** 066501
[12] Safaei S, Galicka M, Kacman P and Buczko R 2015 *New J. Phys.* **17** 063041
[13] Zhou J and Jena P 2017 *Phys. Rev.* B **95** 081102
[14] Murakami S 2006 *Phys. Rev. Lett.* **97** 236805
[15] Liu Z, Liu C-X, Wu Y-S, Duan W-H, Liu F and Wu J 2011 *Phys. Rev. Lett.* **107** 136805
[16] Huang Z-Q, Chuang F-C, Hsu C-H, Liu Y-T, Chang H-R, Lin H and Bansil A 2013 *Phys. Rev.* B **88** 165301
[17] Wang D, Chen L, Liu H and Wang X 2013 *J. Phys. Soc. Japan* **82** 094712
[18] Drozdov I K, Alexandradinata A, Jeon S, Nadj-Perge S, Ji H, Cava R, Bernevig B A and Yazdani A 2014 *Nat. Phys.* **10** 664
[19] Kawakami N, Lin C-L, Kawai M, Arafune R and Takagi N 2015 *Appl. Phys. Lett.* **107** 031602
[20] Yang F *et al* 2012 *Phys. Rev. Lett.* **109** 016801
[21] Taskin A A, Sasaki S, Segawa K and Ando Y 2012 *Phys. Rev. Lett.* **109** 066803
[22] Liu C-X, Zhang H, Yan B, Qi X-L, Frauenheim T, Dai X, Fang Z and Zhang S-C 2010 *Phys. Rev.* B **81** 041307
[23] Hirahara T, Bihlmayer G, Sakamoto Y, Yamada M, Miyazaki H, Kimura S-I, Blügel S and Hasegawa S 2011 *Phys. Rev. Lett.* **107** 166801
[24] Bieniek M, Woźniak T and Potasz P 2017 *J. Phys.: Condens. Matter* **29** 155501
[25] Chen L, Wang Z F and Liu F 2013 *Phys. Rev.* B **87** 235420
[26] Li X, Liu H, Jiang H, Wang F and Feng J 2014 *Phys. Rev.* B **90** 165412
[27] Koroteev Y M, Bihlmayer G, Chulkov E V and Blügel S 2008 *Phys. Rev.* B **77** 045428
[28] Pan H and Wang X-S 2015 *Nanoscale Res. Lett.* **10** 334
[29] Bian G, Wang Z, Wang X-X, Xu C, Xu S, Miller T, Hasan M Z, Liu F and Chiang T-C 2016 *ACS Nano* **10** 3859
[30] Cantele G and Ninno D 2017 *Phys. Rev. Mater.* **1** 014002
[31] Zhang P, Liu Z, Duan W, Liu F and Wu J 2012 *Phys. Rev.* B **85** 201410
[32] Bieniek M, Woźniak T and Potasz P 2016 *Acta Phys. Pol.* A **2** 609
[33] Jin K-H and Jhi S-H 2015 *Sci. Rep.* **5** 8426
[34] Chuang F-C, Hsu C-H, Chen C-Y, Huang Z-Q, Ozolins V, Lin H and Bansil A 2013 *Appl. Phys. Lett.* **102** 022424
[35] Wang D, Chen L, Liu H and Wang X 2014 *Europhys. Lett.* **104** 57011
[36] Eisert J, Cramer M and Plenio M B 2010 *Rev. Mod. Phys.* **82** 277
[37] Amico L, Fazio R, Osterloh A and Vedral V 2008 *Rev. Mod. Phys.* **80** 517
[38] Li H and Haldane F D M 2008 *Phys. Rev. Lett.* **101** 010504
[39] Oliveira T P, Ribeiro P and Sacramento P D 2014 *J. Phys.: Condens. Matter* **26** 425702
[40] Fidkowski L 2010 *Phys. Rev. Lett.* **104** 130502
[41] Fang C, Gilbert M J and Bernevig B A 2013 *Phys. Rev.* B **87** 035119
[42] Turner A M, Zhang Y and Vishwanath A 2010 *Phys. Rev.* B **82** 241102
[43] Hermanns M, Salimi Y, Haque M and Fritz L 2014 *J. Stat. Mech.* P10030
[44] Kargarian M and Fiete G A 2010 *Phys. Rev.* B **82** 085106
[45] Alexandradinata A, Hughes T L and Bernevig B A 2011 *Phys. Rev.* B **84** 195103
[46] Hughes T L, Prodan E and Bernevig B A 2011 *Phys. Rev.* B **83** 245132
[47] Prodan E, Hughes T L and Bernevig B A 2010 *Phys. Rev. Lett.* **105** 115501
[48] Mondragon-Shem I, Khan M and Hughes T L 2013 *Phys. Rev. Lett.* **110** 046806
[49] Mondragon-Shem I and Hughes T L 2014 *Phys. Rev.* B **90** 104204
[50] Liu Y and Allen R E 1995 *Phys. Rev.* B **52** 1566
[51] Slater J C and Koster G F 1954 *Phys. Rev.* **94** 1498
[52] Chadi D J 1977 *Phys. Rev.* B **16** 790
[53] Dziawa P *et al* 2012 *Nat. Mater.* **11** 1023–7
[54] Gonze X *et al* 2016 *Comput. Phys. Commun.* **205** 106
[55] Togo A and Tanaka I 2015 *Scr. Mater.* **108** 1
[56] Parlinski K, Li Z Q and Kawazoe Y 1997 *Phys. Rev. Lett.* **78** 4063
[57] Evarestov R A and Losev M V 2009 *J. Comput. Chem.* **30** 2645
[58] Singh S and Romero A H 2017 *Phys. Rev.* B **95** 165444
[59] Plenio M B and Virmani S 2007 *Quantum Inf. Comput.* **7** 1–51
[60] Peschel I 2003 *J. Phys. A: Math. Gen.* **36** L205
[61] Gioev D and Klich I 2006 *Phys. Rev. Lett.* **96** 100503
[62] Klich I 2006 *J. Phys. A: Math. Gen.* **39** L85
[63] Ryu S and Hatsugai Y 2006 *Phys. Rev.* B **73** 245115
[64] Huang Z and Arovas D P 2012 *Phys. Rev.* B **86** 245109
[65] Liu J and Vanderbilt D 2014 *Phys. Rev.* B **90** 125133
[66] Chandran A, Khemani V and Sondhi S L 2014 *Phys. Rev. Lett.* **113** 060501
[67] Kane C L and Mele E J 2005 *Phys. Rev. Lett.* **95** 226801
[68] Harrison W A 1980 *Electronic Structure and the Properties of Solids* 1st edn (New York: Dover)